

This is the accepted manuscript made available via CHORUS. The article has been published as:

Dynamics of a fractal set of first-order magnetic phase transitions in frustrated  $\text{Lu}_2\text{CoMnO}_6$

Adra Carr, John Bowlan, Claudio Mazzoli, Colby Walker, Xiaxin Ding, Andi Barbour, Wen Hu, Stuart Wilkins, Jong Hyuk Kim, Nara Lee, Young Jai Choi, Shi-Zeng Lin, Richard L. Sandberg, and Vivien S. Zapf

Phys. Rev. B **103**, L060401 — Published 4 February 2021

DOI: [10.1103/PhysRevB.103.L060401](https://doi.org/10.1103/PhysRevB.103.L060401)

# Dynamics of a fractal set of 1st order magnetic phase transitions in frustrated $\text{Lu}_2\text{CoMnO}_6$

Adra Carr,<sup>1,2,\*</sup> John Bowlan,<sup>3,\*</sup> Claudio Mazzoli,<sup>4,\*</sup> Colby Walker,<sup>2,5</sup> Xiabin Ding,<sup>1,†</sup> Andi Barbour,<sup>4</sup> Wen Hu,<sup>4</sup> Stuart Wilkins,<sup>4</sup> Jong Hyuk Kim,<sup>6</sup> Nara Lee,<sup>6</sup> Young Jai Choi,<sup>6</sup> Shi-Zeng Lin,<sup>7</sup> Richard L. Sandberg,<sup>2,5</sup> and Vivien S. Zapf<sup>1</sup>

<sup>1</sup>*National High Magnetic Field Laboratory (NHMFL), Los Alamos National Laboratory (LANL), Los Alamos, New Mexico 87545, USA*

<sup>2</sup>*Center for Integrated Nanotechnologies (CINT), LANL, Los Alamos, New Mexico 87545, USA*

<sup>3</sup>*C-PCS, LANL, Los Alamos, NM 87545*

<sup>4</sup>*NSLS-II, Brookhaven National Laboratory, Upton, New York, USA*

<sup>5</sup>*Department of Physics and Astronomy, Brigham Young University, Provo, Utah, 84602*

<sup>6</sup>*Department of Physics, Yonsei University, Seoul 03722, Korea*

<sup>7</sup>*Theoretical division, LANL, Los Alamos, New Mexico 87545, USA*

(Dated: January 14, 2021)

The Axial Next Nearest Neighbor Ising (ANNNI) model predicts a fractal (infinite) set of phases with incommensurate wave vectors that are separated by 1st order phase boundaries. This complexity results from a simple frustration condition between nearest and next-nearest neighbor interactions along a chain of Ising spins. Using x-ray photon correlation spectroscopy (XPCS), we investigate the surprising antiferromagnetic dynamics that emerge from such a complex phase diagram over a wide range of temperatures. We present XPCS measurements of the frustrated magnetic chain compound  $\text{Lu}_2\text{CoMnO}_6$  and Monte Carlo simulations. Incommensurate magnetic Bragg peaks slide towards commensurate ‘up up down down’ spin order with decreasing temperature and increasing time. Both simulation and experiment support a counter-intuitive ‘upside-down’ temperature dependence of the magnetic dynamics: at higher temperatures in the region of 1st order phase boundaries, slower dynamics are observed where the speckle maintains its coherence. At the lowest temperatures, where part of the sample adopts commensurate order, the dynamics speed up and result in fast decoherence.

In frustrated magnets, seemingly simple competition between spin interactions can create profound complexity. The Axial Next-Nearest Neighbor Ising (ANNNI) model [1–3] is a classic model of frustration in which nearest-neighbor ferromagnetic (FM) interactions and next-nearest-neighbor antiferromagnetic (AFM) interactions compete with each other along chains of Ising spins. As an ANNNI system is cooled below  $T_N$ , it passes through a fractal set of 1st order phase boundaries that separate AFM phases with different incommensurate (ICM) wavevectors, referred to as the ‘Devil’s staircase’ or ‘Devil’s flower’ [1, 2]. At a lower temperature, a CM wave vector emerges such as ‘up up down down’ spin ordering along the chains of Ising spins.

The existence of such a large number 1st order phase transitions should produce interesting dynamics of the magnetic system. However, historically the dynamics of antiferromagnets, frustrated or otherwise, has been difficult to study due to their domains having no net magnetization. Thus, the development of x-ray based techniques at light sources present unique opportunities to probe AFM domain dynamics [4–11]. In particular, x-ray photon correlation spectroscopy (XPCS) of Bragg scattering that is resonantly tuned to magnetic ions can detect AFM order and its inhomogeneities in time (seconds to hours) and space (nanometers to microns)[12–15]. This is important since frustrated systems evolve between different, nearly-degenerate states creating slow dynamics and inhomogeneities. XPCS has led to e.g. observations of the dynam-

ics of spin density waves in Cr [12] and of spin-helix phases in Dy [13, 14]. Thus far, XPCS studies of antiferromagnets have found that when samples are cooled slightly below the Néel temperature  $T < T_N$ , the AFM dynamics become slow or freeze, as would be intuitively expected from thermal activation [12–14].

In this work however, we use XPCS to observe very slow dynamics over a broad range of temperature down to a quarter of  $T_N$  in highly frustrated  $\text{Lu}_2\text{CoMnO}_6$  [16–19]. Moreover, we provide a theoretical framework to understand the dynamics using Monte Carlo simulations of the ANNNI model. This compound is known to be a likely ANNNI system based on previous measurements of thermodynamic properties, muon spin resonance ( $\mu\text{SR}$ ) and neutron diffraction [20, 21].  $\text{Co}^{2+}$  and  $\text{Mn}^{4+}$  with  $S = 3/2$  spins occupy oxygen cages, and the two magnetic ions alternate along the a, b, and c axes [16] with lattice spacing of  $a = 5.1638(1) \text{ \AA}$ ,  $b = 5.5467(1) \text{ \AA}$ ,  $c = 7.4153(1) \text{ \AA}$ . A powder neutron diffraction study found that the magnetic state at 4 K consists of  $\text{Co} \uparrow \text{Mn} \uparrow \text{Co} \downarrow \text{Mn} \downarrow$  with both the spins and wave vector along the c axis, and a slight incommensuration with  $\vec{k} \approx [0.0223(8), 0.0098(7), 0.5]$  (see Fig. 1(a)) [16]. Since the compound is a type II multiferroic [16–19], previous studies used both the magnetization and electric polarization to determine that this system has slow dynamics, down to hour time scales, as well as frequency dependence of the above quantities. These dynamics were observed below

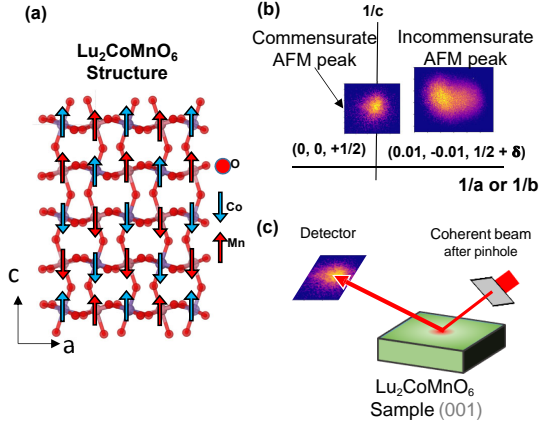


Figure 1. (a) Structure of  $\text{Lu}_2\text{CoMnO}_6$  with spins (arrows) and Lu atoms omitted. (b) Incommensurate (ICM) and commensurate (CM) Bragg peaks, shown with their respective reciprocal space wavevector. (c) Experimental setup of a resonant XPCS experiment, with the  $c$ -axis normal to the illuminated sample face.

$T_N = 48$  K and above  $T_{\text{Hyst}} = 30 - 35$  K where hysteresis emerges in the magnetization and electric polarization on hour timescales. Dynamics between ps and  $\mu\text{s}$  timescales were also uncovered by measuring  $\mu\text{SR}$  and neutron diffraction [21]. Below  $T_{\text{Hyst}}$ , hysteresis appears in the magnetization and electric polarization suggesting that AFM and field-induced FM domains become pinned below this temperature by spin-lattice interactions [16, 19].

XPCS data were collected on a mm-sized single crystal of  $\text{Lu}_2\text{CoMnO}_6$  [18] at the Coherent Soft X-ray Scattering (CSX, 23-ID-1) beamline at NSLS-II [15] during three different beam times. This beamline has previously demonstrated sufficient stability for XPCS studies over multiple hours [15]. All data presented here are for one beamtime and one sample, while data for two additional beamtimes and one additional sample are presented in the S.I. [22] (see, also, references [23–25] therein). The crystal was polished on the (001) faces down to  $0.3 \mu\text{m}$  grit, and mounted with the (001) face upward on a copper sample holder with silver paint. Coherent X-rays passed through a  $10 \mu\text{m}$  pinhole, then resonantly Bragg scattered off the Co or Mn ions in the geometry shown in Fig. 1. Speckle in the Bragg peak was detected using a 2D detector and serves as a measure of AFM inhomogeneities. The autocorrelation function of this speckle can be analyzed to extract statistical information. Each speckle pattern was recorded at a fixed  $T$  every 3.25 s for up to three hours, after verifying thermalization (see S.I.) [22]. The dynamics of the speckle pattern, and thus the domain patterns which they encode, are analyzed by computing the autocorrelation function  $g^{(2)}(\vec{q}, \tau)$  of the speckle

intensity  $I(\vec{q}, t)$ :  $g^{(2)}(\vec{q}, \tau) = \langle I(\vec{q}, t)I(\vec{q}, t + \tau) \rangle / \langle I(\vec{q}, t) \rangle^2$ . Here, the intensities  $I(\vec{q}, t)$  and  $I(\vec{q}, t + \tau)$  are extracted for a particular momentum vector  $\vec{q}$  at times  $t$  and  $t + \tau$ , with  $\tau$  being a delay time and angle brackets denoting time averaging.

We investigate the two satellite ICM Bragg peaks  $\vec{k} = [\pm\delta, \mp\delta, 1/2 \mp \epsilon]$  and a CM Bragg peak  $\vec{k} = [0, 0, 1/2]$ , where the CM peak corresponds to the ‘up up down down’ ordering.  $\delta$  and  $\epsilon$  are in the range of 0.01 or lower and decrease with  $T$  [22]. Data was taken at Co and Mn edges for  $\sigma$  and  $\pi$  X-ray polarization, and a complete XPCS data set was taken at the Co edge with  $\pi$  polarization since it had the largest magnitude.

We find that above  $T_{\text{Hyst}}$  (the region where physical properties have no hysteresis in  $T$  or magnetic field) the nominal CM  $[0, 0, 1/2]$  Bragg peak has no resolvable energy dependence near the Co or Mn  $L_3$  edges, showing that this peak is not at a magnetic resonance. We conclude that it is dominated by the second harmonic of the X-ray beam diffracting off the  $[0, 0, 1]$  lattice peak. However, below  $T_{\text{Hyst}}$  this Bragg peak acquires a strong resonance at the Co and Mn  $L_3$  edges. Thus this Bragg peak becomes dominated by the  $[0, 0, 1/2]$  magnetic peak. The predominance of the spin rather than the charge scattering channel at the lowest temperature is also confirmed by comparing  $\sigma$  and  $\pi$  polarizations (see S.I. [22]). Meanwhile, the ICM peak can be observed only at the Co and Mn  $L_3$  edges at all  $T < T_N$ , both above and below  $T_{\text{Hyst}}$ , proving its magnetic character. The fact that the CM peak abruptly acquires a magnetic component below  $T_{\text{Hyst}}$ , may indicate that part of the sample evolves all the way to the CM order as  $T$  is lowered, while another part of the sample remains trapped in a state described by an ICM wavevector. Evidence for this is also found in intermittent pinning of parts of the ICM peak as the temperature is lowered (see Fig. 1 and movie in S.I.). The wave vectors of the CM and ICM peaks were reproducible at different locations on the sample, though the ICM peaks were not always visible.

We find that for the ICM peak, there is a small  $T$ -dependence of  $\delta$  and  $\epsilon$  (see S.I. [22]) such that the ICM peaks approaches the CM  $\vec{k} = [0, 0, 1/2]$  position as  $T$  is lowered from  $T_N$  to  $T_{\text{Hyst}}$ , as predicted for the ANNNI model. We also noted a significant drift in the magnetic ICM Bragg peak position over time for  $T > T_{\text{Hyst}}$ . This drift is shown in Fig. 2 over a roughly 2 hour period, with a lack of drift in CM peak shown for comparison. A similar drift of the ICM peak towards the CM peak has been observed in the potential ANNNI spin chain compound  $\text{Ca}_3\text{Co}_2\text{O}_6$  [20, 26, 27] where it was attributed to the inability of the system to reach its stable ICM wave vector after a decrease in  $T$  due to very slow dynamics.

Figure 3 (a) and (b) shows the dynamics of speckle in the ICM peak at the Co edge at 778 eV at  $T = 35$  K and 24 K, just

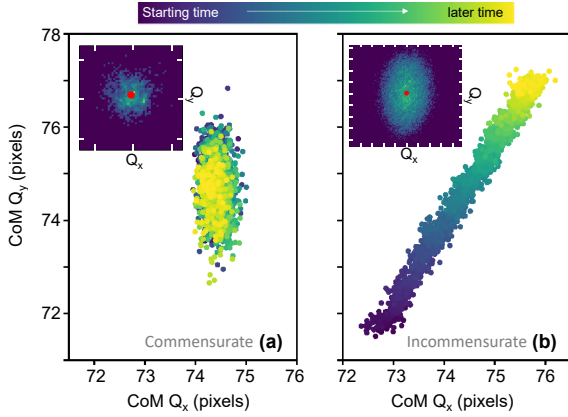


Figure 2. Center of Mass (CoM) of CM (a) and ICM (b) peaks at 35 K shown in detector pixels (1 pixel =  $7 \times 10^{-5} \text{ \AA}^{-1}$ ). The color denotes relative position in time over 1.8 hrs. Insets show the Bragg peak with red dot indicating CoM. White hashmarks denote 20 pixel intervals.

above and below  $T_{\text{Hyst}} = 30 \text{ K}$ . On the right are waterfall plots, showing an average over a vertical stripe through the center of the Bragg peak  $1.4 \times 10^{-4} \text{ \AA}^{-1}$  wide (2 pixels) vs time. The ICM speckle pattern is relatively unchanged at 35 K over the 3 hours, whereas at 25 K the speckle shifts and decorrelates on this timescale.

In Fig. 3 (c) and (d) the normalized intermediate scattering function  $g^{(2)} - 1$  (the autocorrelation function between the signal at different times) is shown at  $T = 25, 35$  and  $55 \text{ K}$ . The CM peak resonates at the Co and Mn edges for 25 K, while the ICM peak resonates at 25 and 35 K. 55 K is above  $T_N$  and therefore no magnetic signal is present in the data while the reported signal in the CM position at this T is attributed to lattice, as already discussed. The autocorrelation is normalized to the average of  $g^{(2)} - 1$  within the first 30 s of integration, serving as a representative baseline. The non-normalized autocorrelation also showed a clear decrease in speckle contrast with decreasing  $T$ , consistent with the emergence of fast ( $\mu\text{s}$ ) relaxation timescales observed in other work [21]. Non-normalized autocorrelations as well as the exact regions of interest (ROIs) used can be found in the S.I. [22]. Autocorrelation functions for other sub-regions of the CM Bragg peak were unable to discern notably separate dynamics between the central and outer portions of the Bragg peak (see S.I. [22]).

Therefore, by means of XPCS we determine that the speckle from domains in the magnetic ICM and CM peaks at 25 K (below  $T_{\text{Hyst}}$ ) decorrelate significantly more rapidly than at 35 K. This result is reproduced in an additional data set shown in the S.I. [22]. While this observation is counter-intuitive since dynamics usually freeze at low  $T$ , it is in fact a prediction of

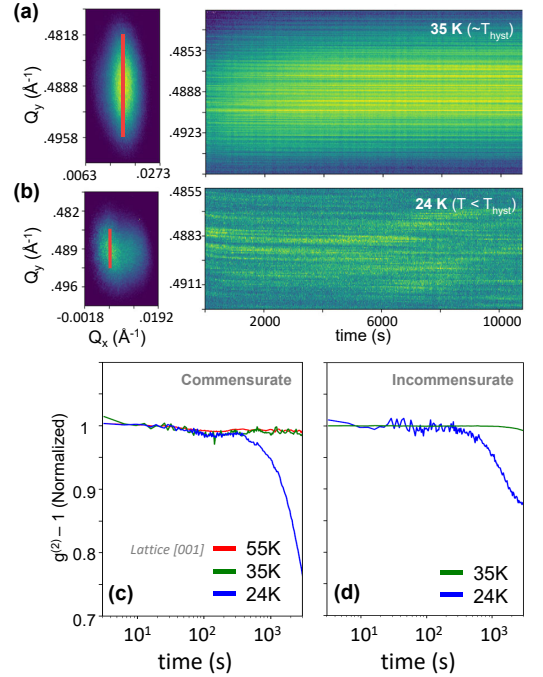


Figure 3. a) (Right) Waterfall plot showing the cross section of a  $\pi$  ICM Bragg peak at 35 K vs time, where cross section is integrated over the red lineout defined on the Left. b) Similar waterfall plot for 24 K. c) Normalized autocorrelation function ( $g^{(2)} - 1$ ) vs. time for the CM peak at  $[0, 0, 1/2]$  and d) ICM peak at  $[0.0087, -0.0042, 0.489]$  and  $[0.0168, -0.006, 0.4888]$  at 35 K. All data is shown for the Co  $L_3$  edge with  $\pi$  polarization. The data at 55 K is above  $T_N$  and thus represents the  $[001]$  structural peak in the first harmonic of the X-ray beam.

the ANNNI model due to the presence of a Devil's staircase of  $1^{\text{st}}$  order phase transitions at intermediate temperatures [1–3]. These dense  $1^{\text{st}}$  order phase boundaries can lead to an effective pinning of ICM wavevectors and consequently slower magnetic dynamics. Below  $T_{\text{Hyst}}$  on the other hand, large stable magnetic domains form and the dynamic speckle behavior is produced by faster local fluctuations within each domain.

In the following, we calculate the dynamics in an ANNNI Monte Carlo model. Monte Carlo simulations of the dynamic behavior of the ANNNI model were performed to compare with the experimental data. We note that in  $\text{Lu}_2\text{CoMnO}_6$  there are two magnetic ions instead of one which is a deviation from the classic single-ion ANNNI model. We perform simulations for the two-ion ANNNI model (here) and compare to the single-ion model (see S.I. [22]) to confirm that the dynamics are similar. Moreover we perform calculations for a 2D and a 3D model (S.I. [22]) and find similar dynamics.

The in-plane ordering wavevector is small, thus we assume

a simple nearest-neighbor FM interaction in the  $a$ - $b$  plane. The spin Hamiltonian is expressed as:

$$\mathcal{H} = -J_1 \sum_{NN} \sigma_i S_j^z - J_2 \sum_{NNN} \sigma_i \sigma_j - J'_2 \sum_{NNN} \mathbf{S}_i \cdot \mathbf{S}_j - A \sum_i (S_i^z)^2,$$

where  $\sigma_j = \pm 1$  is the  $\text{Co}^{2+}$  Ising spin and  $|\mathbf{S}_j| = 1$  is the  $\text{Mn}^{4+}$  Heisenberg spin with an easy axis anisotropy,  $A > 0$ .  $\mathbf{S}_j$  and  $\sigma_j$  form two sublattices of the square lattice, as shown in Fig. 4(a).  $J_1 > 0$  is the nearest-neighbor (NN) FM interaction, and  $J_2 < 0$  and  $J'_2 < 0$  are the next-nearest neighbor (NNN) AFM interaction along the  $c$  axis. We choose  $J_2 = J'_2 = -0.6J_1$  and  $A = J_1$  to match the experimental  $T_N$  and  $T_{\text{Hyst}}$ . We employ a 2-D model corresponding to the  $a$ - $c$  plane of  $\text{Lu}_2\text{CoMnO}_6$  and perform Monte Carlo simulations of  $\mathcal{H}$  with the standard Metropolis algorithm.

The calculated ordering wavevector  $Q$  vs.  $T$  is shown in Fig. 4(a). Because of the finite size effect,  $Q$  changes step-wise with  $T$ . There are peaks in the calculated specific heat when  $Q$  changes, which correspond to the 1<sup>st</sup> order phase transition between different  $Q$  states. The 1<sup>st</sup> order phase transition implies slow dynamics in the ICM phase. For increasing system size,  $Q$  changes quasi-continuously through many weak 1<sup>st</sup> order transitions. To capture the dynamics, we compute the autocorrelation function of the spin structure factor  $S(Q, t) \equiv \langle M_z(Q, t) M_z(-Q, t) \rangle$ , represented as:

$$A(t) = \frac{\int_0^\tau dt_1 (S(t_1) - \bar{S})(S(t + t_1) - \bar{S})}{\int_0^\tau dt_1 (S(t_1) - \bar{S})^2},$$

where  $M_z$  is the  $z$  component of the magnetization at wavevector  $Q$  and  $\langle \dots \rangle$  denotes thermal average. Here  $t$  is the Monte Carlo time and  $\tau$  is the total simulation time, and  $\bar{S}$  is the mean value of  $S(Q, t)$ . The results, displayed in Fig. 4(b), show that the dynamics for  $T_N < T < T_{\text{Hyst}}$  are extremely slow, slower than the region below  $T_{\text{Hyst}}$ . The correlation time is particularly long at the 1st order phase transition point.

The simulations of the dynamics are qualitatively consistent with the XPCS results. The theory and experiment both show ‘inverted’ dynamics, where the speckle decorrelates faster below  $T_{\text{Hyst}}$  than above it.

In conclusion, we observe dynamics of speckle in CM and ICM peaks over a very broad range of temperature down to a quarter of  $T_N$ . Surprisingly, these dynamics are inverted in temperature from ordinary magnets - with fast decorrelation at low  $T$  and slow decorrelation at high  $T$ . Monte Carlo simulations show that these unusual dynamics are predicted by the ANNNI model for both one and two types of magnetic ions. Above  $T_{\text{Hyst}}$  the ANNNI model predicts many (theoretically infinite) first order phase transitions occurring at closely-spaced temperatures whose domain boundaries pin the ICM

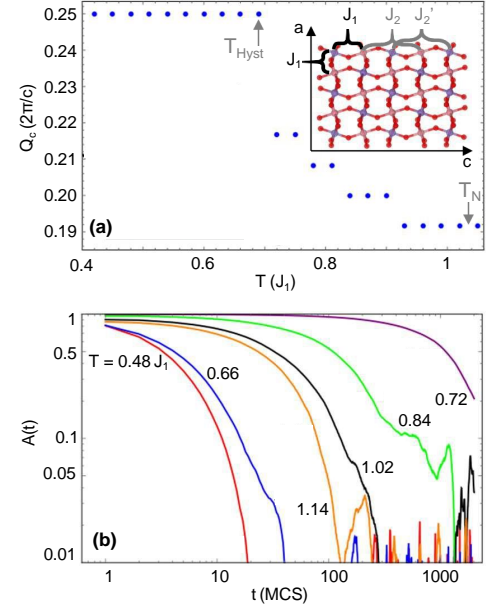


Figure 4. (a) Monte Carlo simulations of the ICM AFM wavevector  $Q$  vs  $T$ , obtained by slowly cooling to  $T = 0$  and then heating. Inset shows the magnetic model with nearest and next-nearest neighbor magnetic interactions. (b) Calculated spin autocorrelation function  $A(t)$  at fixed  $Q = 0.25 \times 2\pi/c$  vs time for varying  $T$ . Time ( $t$ ) is shown in units of Monte Carlo sweep (MCS).

wave vectors, creating slow dynamics. This manifests as a lack of decorrelation in the speckle measured. Though the ICM wave vectors do not decorrelate, they drift in the direction the CM wave vector for at least three hours after a change in  $T$ , as has been seen in other similar ANNNI systems [27]. Below  $T_{\text{Hyst}}$ , the system has stable pinned domains and so the dynamics are dominated by fast fluctuations within each domain and rapid decorrelation of the speckle. Previous XPCS investigations of Dy and Cr also showed ICM order due to frustration between nearest and next-nearest neighbors [12, 14]. However, these systems do not have Ising spins and are thus not examples of the ANNNI model. In these compounds, dynamics were only observed in the immediate vicinity of  $T_N$ .

Our work demonstrates that magnetic frustration can produce unexpected dynamics over a wide range of temperatures detectable by XPCS. Though the ANNNI model of frustration was first developed in the 1980's, we can now investigate its ramifications on the dynamics of antiferromagnetic inhomogeneities using both simulation and experiments.



## ACKNOWLEDGEMENTS

We are grateful to Ashish Tripathi, Benjamin Pound, Shalinee Chikara for helpful experimental aid and to Cristian Batista and Walter Selke for valuable discussions. Scientific work was begun in the LDRD program at LANL and completed - in particular, the theoretical work - as part of the U.S. DOE, Office of Science, Basic Energy Sciences, Materials Sciences and Engineering Division, Condensed Matter Theory Program. This research utilized beamline 23-ID-1 of the NSLS II, a U.S. DOE Office of Science User Facility operated for the DOE Office of Science by Brookhaven National Laboratory under Contract No. DE-SC0012704; as well as the facilities of CINT, an Office of Science User Facility operated for the U.S. DOE Office of Science by LANL; and finally the facilities of the NHMFL, funded by the U.S. NSF through Cooperative Grant No. DMR-1157490, the U.S. DOE and the State of Florida. Sample growth efforts at Yonsei University were supported by the National Research Foundation of Korea Grants NRF-2017R1A5A1014862 (SRC program: vdWMRC center, NRF-2018R1C1B6006859, and NRF-2019R1A2C2002601).

---

\* These authors contributed equally

† Now at: Idaho National Laboratory, Idaho Falls, Idaho

- [1] P. Bak and M. H. Jensen, *J. Phys. C* **13**, L881 (1980).
- [2] P. Bak, *Rep. Prog. Phys.* **45**, 587 (1982).
- [3] W. Selke, *Physics Reports* **170**, 213 (1988).
- [4] M. Schwickert, G. Guo, M. Tomaz, W. O'Brien, and G. Harp, *Phys. Rev. B* **58**, R4289 (1998).
- [5] J. Kortright, D. Awschalom, J. Stöhr, S. Bader, Y. Idzerda, S. Parkin, I. K. Schuller, and H.-C. Siegmann, *J. Magn. Magn. Mat.* **207**, 7 (1999).
- [6] F. Nolting, A. Scholl, and J. Stöhr, *Nature* **405**, 767 (2000).
- [7] J. Stöhr and H. C. Siegmann, *Magnetism: From Fundamentals to Nanoscale Dynamics*, Vol. 1 (SPRINGER, 2006).
- [8] T. Zhao, A. Scholl, F. Zavaliche, K. Lee, M. Barry, A. Doran, M. P. Cruz, Y. H. Chu, C. Ederer, N. A. Spaldin, R. R. Das, D. M. Kim, S. H. Baek, C. B. Eom, and R. Ramesh, *Nature Mat.* **5**, 823 (2006).
- [9] M. G. Kim, H. Miao, B. Gao, S.-W. Cheong, C. Mazzoli, A. Barbour, W. Hu, S. B. Wilkins, I. K. Robinson, M. P. M. Dean, and V. Kiryukhin, *Nature Comm.* **9**, 5013 (2018).
- [10] T. Kołodziej, I. Biało, W. Tabiś, M. Zubko, J. Żukrowski, K. Łątka, J. E. Lorenzo, C. Mazzoli, Z. Kąkol, A. Kozłowski, Z. Tarnawski, E. Wilke, P. Babik, V. Chlan, R. Řezníček, H. Štěpánková, P. Novák, Y. Joly, J. Niewolski, and J. M. Honig, *Phys. Rev. B* **102**, 075126 (2020).
- [11] R. Kukreja, N. Hua, J. Ruby, A. Barbour, W. Hu, C. Mazzoli, S. Wilkins, E. E. Fullerton, and O. G. Shpyrko, *Phys. Rev. Lett.* **121**, 177601 (2018).
- [12] O. G. Shpyrko, E. D. Isaacs, J. M. Logan, Y. Feng, G. Aeppli, R. Jaramillo, H. C. Kim, T. F. Rosenbaum, P. Zschack, M. Sprung, S. Narayanan, and A. R. Sandy, *Nature* **447**, 68 (2006).
- [13] S. Konings, C. Schüßler-Langeheine, H. Ott, E. Weschke, E. Schierle, H. Zabel, and J. B. Goedkoop, *Phys. Rev. Lett.* **106**, 077402 (2011).
- [14] S.-W. Chen, H. Guo, K. A. Seu, K. Dumesnil, S. Roy, and S. K. Sinha, *Phys. Rev. Lett.* **110**, 217201 (2013).
- [15] X. M. Chen, V. Thampy, C. Mazzoli, A. M. Barbour, H. Miao, G. D. Gu, Y. Cao, J. M. Tranquada, M. P. M. Dean, and S. B. Wilkins, *Phys. Rev. Lett.* **117**, 167001 (2016).
- [16] S. Yáñez-Vilar, E. D. Mun, V. S. Zapf, B. G. Ueland, J. S. Gardner, J. D. Thompson, J. Singleton, M. Sánchez-Andújar, J. Mira, N. Biskup, M. A. Señarís-Rodríguez, and C. D. Batista, *Phys. Rev. B* **84**, 134427 (2011).
- [17] N. Lee, H. Y. Choi, Y. J. Jo, M. S. Seo, S. Y. Park, and Y. J. Choi, *Applied Physics Letters* **104**, 112907 (2014).
- [18] S. Chikara, J. Singleton, J. Bowlan, D. A. Yarotski, N. Lee, H. Y. Choi, Y. J. Choi, and V. S. Zapf, *Phys. Rev. B* **93**, 180405 (2016).
- [19] H. Y. Choi, J. Y. Moon, J. H. Kim, Y. J. Choi, and N. Lee, *Crystals* **7** (2017).
- [20] Y. Kamiya and C. D. Batista, *Phys. Rev. Lett.* **109**, 067204 (2012).
- [21] V. S. Zapf, B. G. Ueland, M. Laver, M. Lonsky, M. Pohlitz, J. Müller, T. Lancaster, J. S. Möller, S. J. Blundell, J. Singleton, J. Mira, S. Yáñez Vilar, and M. A. Señarís Rodríguez, *Phys. Rev. B* **93**, 134431 (2016).
- [22] Supplementary Information at [URL will be inserted by publisher] contains discussion of experimental details, heat capacity data, additional XPCS data and analysis such as details of the ROIs, energy-dependencies of scattering peaks, a second set of XPCS data taken in a separate beamtime, and finally additional Monte Carlo simulations for the single-ion model and for a 3D case.
- [23] C. Detlefs, M. Sanchez del Rio, and C. Mazzoli, *European Physical Journal Special Topics* **208**, 359 (2012), [arXiv:1106.4446 \[cond-mat.str-el\]](https://arxiv.org/abs/1106.4446).
- [24] N. Otsu, *IEEE Transactions on Systems, Man, and Cybernetics* **9**, 62 (1979).
- [25] L. T. Coutrim, D. Rigitano, C. Macchiutti, T. J. A. Mori, R. Lora-Serrano, E. Granado, E. Sadrollahi, F. J. Litterst, M. B. Fontes, E. Baggio-Saitovitch, E. M. Bittar, and L. Bufaiçal, *Phys. Rev. B* **100**, 054428 (2019).
- [26] T. Moyoshi, R. Takahashi, and K. Motoya, *J. Phys.: Conf. Series* **273**, 012125 (2011).
- [27] S. Agrestini, C. L. Fleck, L. C. Chapon, C. Mazzoli, A. Bombardi, M. R. Lees, and O. A. Petrenko, *Phys. Rev. Lett.* **106**, 197204 (2011).